Research Article Vol. 9, No. 9 / September 2022 / Optica 987

OPTICA

Controlling the polarization and phase of high-order harmonics with a plasmonic metasurface

Sohail A. Jalil,[1] Kashif M. Awan,[2] Idriss A. Ali,[1] Sabaa Rashid,[3] Joshua Baxter,[3,4] Aleksey Korobenko,[1] Guilmot Ernotte,[1] Andrei Naumov,[1] David M. Villeneuve,[1] André Staudte,[1] Pierre Berini,[3,4,5] Lora Ramunno,[3,4] and Giulio Vampa[1,*]

[1]Joint Attosecond Science Laboratory, National Research Council of Canada and University of Ottawa, Ottawa, Ontario K1N 0R6, Canada
[2]Stewart Blusson Quantum Matter Institute, University of British Columbia, Vancouver, British Columbia V6T 1Z4, Canada
[3]Centre for Research in Photonics, University of Ottawa, 25 Templeton Street, Ottawa, Ontario K1N 6N5, Canada
[4]Department of Physics, University of Ottawa, 150 Louis Pasteur, Ottawa, Ontario K1N 6N5, Canada
[5]School of Electrical Engineering and Computer Science, University of Ottawa, 800 King Edward Avenue, Ottawa, Ontario K1N 6N5, Canada
*Corresponding author: gvampa@uottawa.ca

Received 18 May 2022; revised 5 August 2022; accepted 6 August 2022; published 24 August 2022

Nanostructured surfaces, or metasurfaces, allow exquisite control of linear and nonlinear optical processes by reshaping the amplitude, phase, and polarization of electric and magnetic fields near wavelength-scale heterogeneities. Recently, metasurfaces have broken new ground in high-field attosecond science where they have been utilized to amplify the emission of high-order harmonics of femtosecond infrared laser pulses, a notoriously inefficient process, by enhancing the incident field, and to shape the emitted high harmonics in space. Here we show control of the polarization and phase of high harmonics with a plasmonic metasurface. We design and fabricate perpendicularly aligned rectangular gold antennas on a silicon crystal that generate circularly polarized deep-ultraviolet high harmonics, from a circularly polarized infrared driver, providing a simple path for achieving circular emission from patterned crystals. Our metasurface enhances the circularly polarized harmonics up to ∼43 times when compared to the unpatterned surface, where harmonics are quenched. Looking forward, circularly polarized high harmonics will be useful tools for sensing chiral laser–matter interactions and magnetic materials. Our approach paves the way for polarization control at even shorter, extreme ultraviolet, wavelengths.

https://doi.org/10.1364/OPTICA.464445

1. INTRODUCTION

High-harmonic generation (HHG) is an extremely nonlinear optical process that converts low-energy photons into high-energy ones during interaction with gases [1], liquids [2], and solids [3]. Solid-state HHG has been reported from high-density bulk dielectrics [4,5], semiconductors [3,6], single crystal metals [7], and 2D materials [8], as well as from nanostructured surfaces [9–18]. The latter showcases the flexibility of tailoring the nonlinear optical properties with nano-structuring, opening new research opportunities at the confluence of attosecond science and nanophotonics [19–21].

The effect of nanostructures on solid-state HHG is twofold. First, each individual nanoscale feature enhances the laser electric field and thereby the local HHG efficiency. Such nanostructures have been shown to enhance HHG from sapphire–metal nanocones [9], ZnO cones and ridges [10], plasmonic Au antennas on Si [11], GaP antennas [15], Fano-resonance structures [12], metasurfaces supporting optical bound states in the continuum [16], and epsilon near zero material [13]. Second, far-field emission profiles of the high harmonics can be controlled by arranging the location of individual nanostructures [10]. For instance, focusing harmonics to the diffraction limit has been achieved with Fresnel zone plates [10,17]. More recently, controlled diffraction of extreme ultraviolet (XUV) high harmonics at a photon energy of 11 eV has been achieved with a nanostructured MgO surface [18]. We note that the aforementioned experiments generated linearly polarized harmonics in the UV or XUV regime.

On the other hand, circularly polarized high harmonics are a promising tool for probing magnetic properties of solids [22,23] and chirality-sensitive laser–matter interaction [24,25]. However, a circularly polarized driver cannot produce circularly polarized high harmonics from a gas target because the electrons cannot recollide with the parent ion [26]. More sophisticated engineered optical fields can avoid this problem [27–30]. Some crystals can also produce circularly polarized high harmonics [5,31]. An alternative approach to control polarization of emitted harmonics is using nanostructured metasurfaces. Metasurfaces have been utilized to shape the polarization of low-order perturbative harmonics in the visible and infrared spectral regions [32–35]. In this context, the Pancharatnam–Berry phase, or *geometric* phase, method allows a continuous variation of the nonlinear phase, and thus of

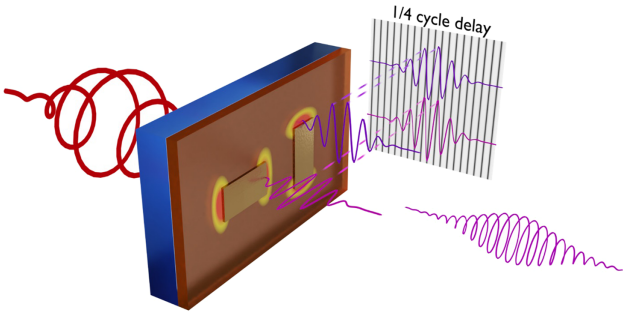

Fig. 1. Concept of the experiment: each antenna resonates for the linear component of the incident circularly polarized driving field that aligns parallel to the antenna's major axis, thereby emitting linearly polarized odd-order high-harmonic radiation with half-cycle multiples of one quarter-cycle delay. Interference of pairs of antennas' emission results in circularly polarized high harmonics upon diffraction. The experiments are performed in reflection; however, transmission geometry is shown for clarity.

the polarization, across the metasurface by simply rotating the individual nanoscale elements [36].

Here we merge the metasurface approach with non-perturbative HHG. Inspired by the geometric phase approach, and by the sensitivity of plasmonic rectangular nano-antennas to the orientation of incident linear polarization relative to the antennas' major axes [11], we design a plasmonic metasurface that controls the polarization of emitted HHG in space. Specifically, we generate circularly polarized harmonics by shining a circularly polarized driver on an array of pairs of rectangular antennas fabricated on a Si substrate, with the major axis of each antenna in the pairs aligned perpendicularly to one another. As sketched in Fig. 1, each antenna couples to the component of the driver's electric field that aligns with the antenna's major axis, effectively linearizing the driver's polarization in each antenna's hotspot and resulting in efficient, enhanced, local high-harmonic emission. Crucially, each antenna emission is synchronized with the driving laser but with a relative phase of $n\pi/2$ ("n" is the harmonic order), determined by the relative orientation of the two antennas. The circularly polarized driver guarantees efficient coupling to both antennas. Therefore, overlapping the linear high-harmonic emissions from the two perpendicular antennas in the far-field results in circularly polarized odd-order harmonics. A similar scheme for bow-tie antennas was proposed in [37].

2. HIGH-HARMONIC GENERATION, DETECTION, AND CHARACTERIZATION

The optical setup for generating and detecting high harmonics is shown in Fig. 2. A titanium sapphire femtosecond regenerative amplifier (Coherent Legend) pumps an optical parametric amplifier (OPA TOPAS, Light Conversion) with an energy of 1.3 mJ/pulse. The OPA delivers signal (1.31 μm wavelength) and idler (2.05 μm wavelength) infrared laser pulses of 80 fs duration at 1 kHz repetition rate. The idler beam, with an energy of ∼200 μJ, is spatially filtered with a diamond pinhole of 100 μm diameter, collimated with a CaF_2 lens, and refocused onto the sample with a spherical focusing mirror of 100 mm focal length. The beam waist on the sample is measured with knife-edge method and is found to be comparable to the size of a patterned nano-antenna array (70 μm). We estimate that a total of ∼20,000 antennas are

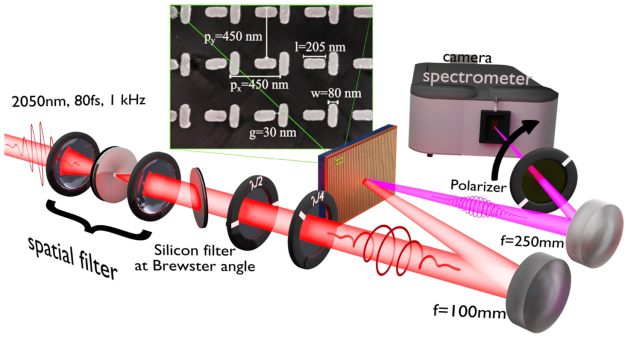

Fig. 2. Experimental setup and scanning electron microscope image (SEM): femtosecond laser pulses with center wavelength of 2050 nm, 80 fs pulse duration at a 1 kHz repetition rate are spatially filtered and focused with a spherical mirror ($f = 100$ mm) on an array of gold antennas fabricated on silicon crystal. A combination of wave plates [half- ($\lambda/2$) and quarter-wave plates ($\lambda/4$)] is utilized to control the laser polarization onto the sample. The polarization of the harmonics generated from the antenna arrays is analyzed using a polarizer suitable for the harmonic wavelengths. High harmonics are collected in reflection geometry and focused with a 250 mm spherical mirror on the slit of the spectrometer (Princeton Instruments Isoplane 320). The inset shows a high-resolution SEM image of perpendicular antennas. The horizontal antenna's major axis is aligned along the [110] direction of the Si crystal. The length, width, gap, pitch, and height of the arrays determine the resonant wavelength.

illuminated simultaneously. A silicon filter is used at the Brewster angle to remove any spurious wavelength coming from the OPA. An iris placed before the spatial filter attenuates and controls the average power of the laser system. A zero-order half-wave plate controls the linear polarization, while a quarter-wave plate ($\lambda/4$) converts the linear polarization to circular polarization. The angle between the incident beam and sample is kept less than ∼ 5 degrees to maximize the resonance.

The sample consists of Au nano-antennas deposited on a single crystal Si film epitaxially grown on a sapphire substrate, R-plane. The inset shows a high-resolution scanning electron image of the rectangular antennas, which are fabricated by electron-beam lithography (see Supplement 1 for details on the fabrication). The nano-antennas are designed to resonate at the laser wavelength (see Supplement 1 for resonance plots and field enhancement), using commercially available finite difference time-domain software from Lumerical. The horizontal nano-antennas are patterned parallel to the [110] direction of the silicon crystal.

The harmonics are measured in reflection to avoid the birefringence of sapphire. The harmonics reflected from the sample are collected and refocused using a spherical mirror (250 mm focal length) onto the slit of a commercial UV-VIS spectrometer (Princeton Instruments Isoplane 320, equipped with a PI-MAX4 ICCD camera). The circularity of the emitted harmonics from antennas and bulk was characterized by rotating an ultra-broadband wire-grid polarizer (250–4000 nm) placed after the sample.

3. RESULTS

Figure 3 shows a comparison between the high-harmonic spectrum produced by nano-antennas and by unpatterned (bulk) Si using circularly polarized (a) and horizontal linearly polarized (b) incident light. The emission extends from the fifth to ninth harmonics

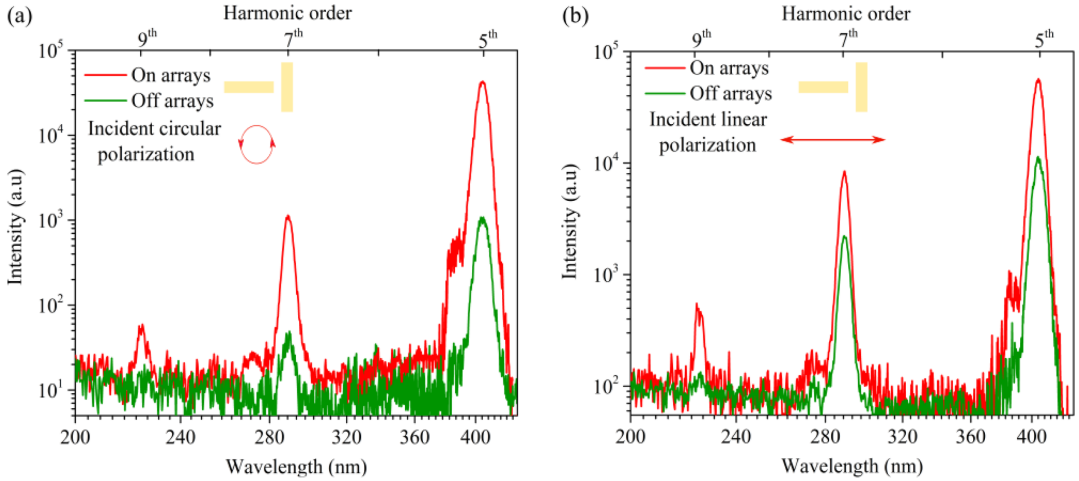

Fig. 3. High-harmonic spectrum with circular and linearly polarized infrared driving field: (a) odd-order high-harmonic generation extending up to the ninth harmonic, when bulk (off arrays, green line) and antennas (on arrays, red line) are driven with a circular polarization at the vacuum intensity of 2.5×10^{10} W cm^{-2}. All the harmonics from arrays are significantly enhanced compared to unpatterned material. (b) A comparison of high-harmonic generation from patterned arrays and unpatterned silicon when the incident polarization is linear and parallel to the major axis of the horizontal antenna (inset). The on/off array contrast is much lower as compared to the circular driving field because bulk emission is significantly suppressed for circular polarization.

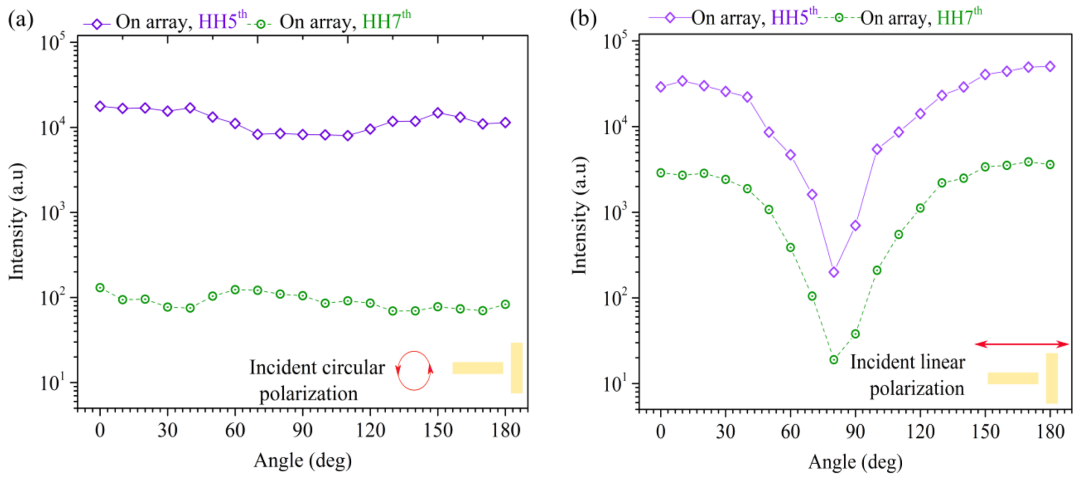

Fig. 4. Polarization analysis of high harmonics illuminated with circularly and linearly polarized infrared driving fields: both panels show harmonic power as a function of the rotation angle of the polarizer. (a) Characterization of harmonics when the array is driven with circular polarization. Fifth and seventh harmonics show little variation, suggesting that the harmonic polarization is circular. (b) Characterization of fifth and seventh harmonics when the array is driven with linear polarization. Harmonic power shows a strong minimum, indicating that the harmonics are linearly polarized.

for an incident intensity (in vacuum) of 2.5×10^{10} W cm^{-2}. The 11th harmonic, at 185 nm, lies beyond the detectable spectral range of our experimental setup. For circular incident polarization, harmonic power from the nano-antennas (red line) is ~43 and ~20 times stronger than from unpatterned Si (green line) at the fifth and seventh harmonics, respectively. This large contrast is due primarily to the quenching of bulk emission from Si with circular input polarization, as can be seen comparing the green lines in (a) and (b). It is known that gas-phase high harmonics are suppressed with circular input polarization because electron trajectories miss the parent ion for re-collision [26]. Many solids behave similarly to gases [3]. Emission from the antennas, on the other hand, remains strong, largely irrespective of the input polarization. This suggests that the polarization inside the plasmonic hotspot is linearized, which keeps high-harmonic emission active. Enhancement from the array using linearly polarized light is 20%–30% weaker than we measured previously [11], largely because of the wider unit cell. Fabrication imperfections may also contribute to the difference.

To confirm that the nano-antennas generate circularly polarized high harmonics in the far field, we analyze their polarization state with a polarizer placed after the sample. Figure 4(a) shows the harmonic power from the nano-antenna arrays, as a function of the polarizer rotation angle, when the polarization of the driving field is kept circular. Clearly, the fifth and seventh harmonics appear to be circularly polarized. On the contrary, when the polarization of the driver is linear and horizontal [Fig. 4(b)], the harmonics show a strong minimum for vertical polarization, indicating that they are horizontally linearly polarized, like the driver. This also confirms that the harmonics have a defined polarization (i.e., they are not unpolarized). Further proof that the harmonics are polarized is shown in Supplement 1 (for the fifth harmonic).

4. DISCUSSION

In conclusion, we demonstrated a plasmonic metasurface that emits circularly polarized high harmonics by exploiting the relative delay between the resonance of two perpendicularly aligned rectangular nano-antennas and the selective enhancement of specific driver polarization states. Adding phase and polarization control to high-harmonic emission from nanostructured surfaces completes previous demonstrations of field-enhanced high-harmonic emission from sub-wavelength nano-structures with the addition of the temporal aspect that is so crucial to all attosecond and high-field phenomena.

Control of the polarization occurs *in situ*, while the high harmonics are being generated, without requiring external optical elements, whose dispersion is a hurdle to the synthesis of femtosecond deep-UV pulses, or tailored light fields. This advantage becomes paramount at even shorter wavelengths, such as for XUV harmonics that can be generated from dielectric crystals, where polarization optics perform poorly or are nonexistent altogether. With the recent demonstration of high-harmonic emission from ceramic plasmonic metals at laser intensities comparable to the damage threshold of dielectrics [7], we foresee the integration of plasmonic metasurfaces on dielectric substrates, for the generation and control, in both amplitude and polarization, of XUV harmonics, and even their extension to frequency combs for ever more precise metrology.

Finally, our metasurface approach provides the opportunity to integrate other functionalities, such as *in situ* focusing of the circularly polarized harmonics [38], and structuring of the polarization in space. With such control in a small-scale deep-UV focus, one can envision revealing magnetic and chiral anisotropy on chemisorbed molecules for catalysis and other energy technologies, where specific chemical bonds can be accessed with deep- and vacuum-UV harmonics.

Funding. SiEPIC Fab; Advanced Nanofab Facility of the Stewart Blusson Quantum Matter Institute, University of British Columbia; Joint Center for Extreme Photonics.

Acknowledgment. The authors thank David Crane and Ryan Kroeker for providing continuing technical support. G. Vampa and S.A. Jalil acknowledge financial support from the Joint Centre for Extreme Photonics. K.M. Awan acknowledges the support of the Advanced Nanofab Facility of the Stewart Blusson Quantum Matter Institute and SiEPIC Fab for fabrication of the plasmonic array sample.

G.V. conceived the experiments, S.A.J., I.A.A., and J.B. performed the simulations, and K.M.A. and S.R. fabricated the sample. G.V., A.K., and G.E. assisted in building the setup and optical measurements, S.A.J. and I.A.A. performed the optical measurements, and S.A.J., G.V., and I.A. analyzed the data. G.V., D.M.V., A.S., A.N., L.R., and P.B. supervised the project, and all authors contributed to the paper.

Disclosures. The authors declare no conflicts of interest.

Data availability. Data underlying the results presented in this paper are not publicly available at this time but may be obtained from the authors upon reasonable request.

Supplemental document. See Supplement 1 for supporting content.

REFERENCES

1. M. Ferray, A. L'Huillier, X. Li, L. Lompre, G. Mainfray, and C. Manus, "Multiple-harmonic conversion of 1064 nm radiation in rare gases," J. Phys. B **21**, L31–L35 (1988).
2. T. T. Luu, Z. Yin, A. Jain, T. Gaumnitz, Y. Pertot, J. Ma, and H. J. Wörner, "Extreme–ultraviolet high–harmonic generation in liquids," Nat. Commun. **9**, 3723 (2018).
3. S. Ghimire, A. D. DiChiara, E. Sistrunk, P. Agostini, L. F. DiMauro, and D. A. Reis, "Observation of high-order harmonic generation in a bulk crystal," Nat. Phys. **7**, 138–141 (2011).
4. T. T. Luu, M. Garg, S. Y. Kruchinin, A. Moulet, M. T. Hassan, and E. Goulielmakis, "Extreme ultraviolet high-harmonic spectroscopy of solids," Nature **521**, 498–502 (2015).
5. Y. S. You, D. A. Reis, and S. Ghimire, "Anisotropic high-harmonic generation in bulk crystals," Nat. Phys. **13**, 345–349 (2017).
6. M. Hohenleutner, F. Langer, O. Schubert, M. Knorr, U. Huttner, S. W. Koch, M. Kira, and R. Huber, "Real-time observation of interfering crystal electrons in high-harmonic generation," Nature **523**, 572–575 (2015).
7. A. Korobenko, S. Saha, A. T. Godfrey, M. Gertsvolf, A. Y. Naumov, D. M. Villeneuve, A. Boltasseva, V. M. Shalaev, and P. B. Corkum, "High-harmonic generation in metallic titanium nitride," Nat. Commun. **12**, 4981 (2021).
8. H. Liu, Y. Li, Y. S. You, S. Ghimire, T. F. Heinz, and D. A. Reis, "High-harmonic generation from an atomically thin semiconductor," Nat. Phys. **13**, 262–265 (2017).
9. S. Han, H. Kim, Y. W. Kim, Y.-J. Kim, S. Kim, I.-Y. Park, and S.-W. Kim, "High-harmonic generation by field enhanced femtosecond pulses in metal-sapphire nanostructure," Nat. Commun. **7**, 13105 (2016).
10. M. Sivis, M. Taucer, G. Vampa, K. Johnston, A. Staudte, A. Y. Naumov, D. Villeneuve, C. Ropers, and P. Corkum, "Tailored semiconductors for high-harmonic optoelectronics," Science **357**, 303–306 (2017).
11. G. Vampa, B. Ghamsari, S. Mousavi Siadat, T. Hammond, A. Olivieri, E. Lisicka-Skrek, A. Y. Naumov, D. Villeneuve, A. Staudte, and P. Berini, "Plasmon-enhanced high-harmonic generation from silicon," Nat. Phys. **13**, 659–662 (2017).
12. H. Liu, C. Guo, G. Vampa, J. L. Zhang, T. Sarmiento, M. Xiao, P. H. Bucksbaum, J. Vučković, S. Fan, and D. A. Reis, "Enhanced high-harmonic generation from an all-dielectric metasurface," Nat. Phys. **14**, 1006–1010 (2018).
13. Y. Yang, J. Lu, A. Manjavacas, T. S. Luk, H. Liu, K. Kelley, J.-P. Maria, E. L. Runnerstrom, M. B. Sinclair, and S. Ghimire, "High-harmonic generation from an epsilon-near-zero material," Nat. Phys. **15**, 1022–1026 (2019).
14. H. Liu, G. Vampa, J. L. Zhang, Y. Shi, S. Buddhiraju, S. Fan, J. Vuckovic, P. H. Bucksbaum, and D. A. Reis, "Beating absorption in solid-state high harmonics," Commun. Phys. **3**, 1–6 (2020).
15. M. R. Shcherbakov, H. Zhang, M. Tripepi, G. Sartorello, N. Talisa, A. AlShafey, Z. Fan, J. Twardowski, L. A. Krivitsky, and A. I. Kuznetsov, "Generation of even and odd high harmonics in resonant metasurfaces using single and multiple ultra-intense laser pulses," Nat. Commun. **12**, 4185 (2021).
16. G. Zograf, K. Koshelev, A. Zalogina, V. Korolev, R. Hollinger, D.-Y. Choi, M. Zuerch, C. Spielmann, B. Luther-Davies, and D. Kartashov, "High-harmonic generation from resonant dielectric metasurfaces empowered by bound states in the continuum," ACS Photon. **9**, 567–574 (2022).
17. D. Gauthier, S. Kaassamani, D. Franz, R. Nicolas, J.-T. Gomes, L. Lavoute, D. Gaponov, S. Février, G. Jargot, and M. Hanna, "Orbital angular momentum from semiconductor high-order harmonics," Opt. Lett. **44**, 546–549 (2019).
18. A. Korobenko, S. Rashid, C. Heide, A. Y. Naumov, D. Reis, P. Berini, P. Corkum, and G. Vampa, "Generation of structured coherent extreme ultraviolet beams from an MgO crystal," Opt. Express **29**, 24161–24168 (2021).
19. N. Yu, P. Genevet, M. A. Kats, F. Aieta, J.-P. Tetienne, F. Capasso, and Z. Gaburro, "Light propagation with phase discontinuities: generalized laws of reflection and refraction," Science **334**, 333–337 (2011).
20. X. Ni, N. K. Emani, A. V. Kildishev, A. Boltasseva, and V. M. Shalaev, "Broadband light bending with plasmonic nanoantennas," Science **335**, 427 (2012).
21. N. Yu and F. Capasso, "Flat optics with designer metasurfaces," Nat. Mater. **13**, 139–150 (2014).
22. J. Stöhr, Y. Wu, B. Hermsmeier, M. Samant, G. Harp, S. Koranda, D. Dunham, and B. Tonner, "Element-specific magnetic microscopy with circularly polarized x-rays," Science **259**, 658–661 (1993).
23. S. Zayko, O. Kfir, M. Heigl, M. Lohmann, M. Sivis, M. Albrecht, and C. Ropers, "Ultrafast high-harmonic nanoscopy of magnetization dynamics," Nat. Commun. **12**, 6337 (2021).
24. N. Böwering, T. Lischke, B. Schmidtke, N. Müller, T. Khalil, and U. Heinzmann, "Asymmetry in photoelectron emission from chiral molecules induced by circularly polarized light," Phys. Rev. Lett. **86**, 1187–1190 (2001).

25. T. Heinrich, M. Taucer, O. Kfir, P. Corkum, A. Staudte, C. Ropers, and M. Sivis, "Chiral high-harmonic generation and spectroscopy on solid surfaces using polarization-tailored strong fields," Nat. Commun. **12**, 3723 (2021).
26. K. Budil, P. Salières, A. L'Huillier, T. Ditmire, and M. Perry, "Influence of ellipticity on harmonic generation," Phys. Rev. A **48**, R3437–R3440 (1993).
27. D. B. Milošević, W. Becker, and R. Kopold, "Generation of circularly polarized high-order harmonics by two-color coplanar field mixing," Phys. Rev. A **61**, 063403 (2000).
28. O. Kfir, P. Grychtol, E. Turgut, R. Knut, D. Zusin, D. Popmintchev, T. Popmintchev, H. Nembach, J. M. Shaw, and A. Fleischer, "Generation of bright phase-matched circularly-polarized extreme ultraviolet high harmonics," Nat. Photonics **9**, 99–105 (2015).
29. D. D. Hickstein, F. J. Dollar, P. Grychtol, J. L. Ellis, R. Knut, C. Hernández-García, D. Zusin, C. Gentry, J. M. Shaw, and T. Fan, "Non-collinear generation of angularly isolated circularly polarized high harmonics," Nat. Photonics **9**, 743–750 (2015).
30. L. Hareli, G. Lerner, O. Cohen, and A. Bahabad, "Circularly polarized high harmonic generation through virtual circular birefringence," Appl. Phys. Lett. **118**, 221106 (2021).
31. D. Baykusheva, A. Chacón, J. Lu, T. P. Bailey, J. A. Sobota, H. Soifer, P. S. Kirchmann, C. Rotundu, C. Uher, and T. F. Heinz, "All-optical probe of three-dimensional topological insulators based on high-harmonic generation by circularly polarized laser fields," Nano Lett. **21**, 8970–8978 (2021).
32. M. Tymchenko, J. S. Gomez-Diaz, J. Lee, N. Nookala, M. A. Belkin, and A. Alù, "Gradient nonlinear Pancharatnam-Berry metasurfaces," Phys. Rev. Lett. **115**, 207403 (2015).
33. G. Li, S. Chen, N. Pholchai, B. Reineke, P. W. H. Wong, E. Y. B. Pun, K. W. Cheah, T. Zentgraf, and S. Zhang, "Continuous control of the nonlinearity phase for harmonic generations," Nat. Mater. **14**, 607–612 (2015).
34. R. Camacho-Morales, M. Rahmani, S. Kruk, L. Wang, L. Xu, D. A. Smirnova, A. S. Solntsev, A. Miroshnichenko, H. H. Tan, and F. Karouta, "Nonlinear generation of vector beams from AlGaAs nanoantennas," Nano Lett. **16**, 7191–7197 (2016).
35. G. Li, S. Zhang, and T. Zentgraf, "Nonlinear photonic metasurfaces," Nat. Rev. Mater. **2**, 17010 (2017).
36. A. Karnieli, Y. Li, and A. Arie, "The geometric phase in nonlinear frequency conversion," Front. Phys. **17**, 1–31 (2022).
37. A. Husakou, F. Kelkensberg, J. Herrmann, and M. Vrakking, "Polarization gating and circularly-polarized high harmonic generation using plasmonic enhancement in metal nanostructures," Opt. Express **19**, 25346–25354 (2011).
38. N. Segal, S. Keren-Zur, N. Hendler, and T. Ellenbogen, "Controlling light with metamaterial-based nonlinear photonic crystals," Nat. Photonics **9**, 180–184 (2015).